Ground State Property Calculations of LiH_n Complexes using IBM Qiskit's Quantum Simulator

B. Avramidis,[1,2] H. P. Paudel,[3] D. Alfonso,[1] Y. Duan,[1] and K.D. Jordan[2]

[1)] *National Energy Technology Laboratory, United States Department of Energy, Pittsburgh, PA 15234, USA*

[2)] *Chemistry Department, University of Pittsburgh, 219 Parkman Ave, Pittsburgh, PA 15260, USA*

[3)] *NETL Support Contractor, 626 Cochrans Mill Road, Pittsburgh, PA 15236-0940, USA*

(*Electronic mail: bavramidis@pitt.edu.)

(Dated: 20 November 2023)

In this study, the variational quantum eigensolver (VQE) on a quantum simulator is used in calculating ground state electronic structure properties of the LiH_n, n = 1 - 3, complexes including their singly charged ions. Results calculated using classical electronic structure algorithms are also included. We investigate the use of the unitary coupled cluster with singles and doubles (UCCSD) ansatz using VQE within Qiskit, and compare results to full configuration interaction (FCI) calculations. Computed ground state energies, electron affinities, ionization potentials and dipole moments are considered. We report the first of its kind simulated quantum computing results of selected LiH_n species, and use the Parity orbital to qubit mapping scheme. We find that VQE / UCCSD results are comparable to classical coupled cluster with singles and doubles (CCSD) for all considered systems with respect to FCI. A VQE calculation cost evaluation is included in which we evaluate performance using both Jordan-Wigner and Parity orbital to qubit mapping schemes. We also discuss some of the current limitations of utilizing VQE for the study of chemical systems.

I. INTRODUCTION:

Accurate wave function based electronic structure calculations demonstrate a steep scaling with respect to the number of electrons and the size of the basis set used. For example, coupled cluster with singles, doubles and perturbative triples (CCSD(T)) calculations scale as n^7, where n corresponds to the number of electrons[1]. While some algorithms may demonstrate better scaling, this is at the cost of introducing approximations[2]. For this reason there is considerable interest in the idea proposed by Feynman in 1981[3] to use computers built upon the principles of quantum mechanics to simulate quantum systems.

The field of Quantum Information Science (QIS)[4,5] ascribes its existence to studies[6–10], showing that some quantum algorithms scale significantly better than their classical counterparts. These results spurred on the development of quantum computers which have been theoretically shown to scale advantageously with respect to system size compared to the computational cost associated in using classical electronic structure programs[11–14].

While the development of devices capable of representing qubits has been a great engineering and scientific achievement, a long term quantum computing (QC) realization has faced challenges in manufacturing and implementing full scale quantum computers with a substantial number of qubits required to represent large, complex quantum systems. Nevertheless, companies have made progress in this area and further advancements in short-term quantum computing capabilities should be expected for years to come. For example, IBM announced a 433 qubit device in November of 2022, with plans to develop a 1,000+ qubit quantum computer in 2023 and a device with 4,000+ qubits by 2025[15,16].

The effects of noise due to thermal environments and other difficult to control phenomena has led researchers to label current quantum computers as noisy intermediate-scale quantum (NISQ) systems, and many algorithms have been developed for use on these systems[17,18]. Though these achievements are promising with respect to the future of QIS within the NISQ era, applications of quantum computing in solving electronic structure problems for even the smallest of molecules using a flexible basis sets require resources beyond those currently available. As an alternative, the availability of quantum simulators has made running NISQ era quantum computing algorithms available to the general public. An example is IBM's Qiskit module which has been interfaced with Python coding language[19,20].

In our previous study[21], by using quantum algorithms we have described the reaction and vibrational energetics of the CO2-NH3 interaction. In this study we further explore the computational capabilities of the hybrid quantum - classical algorithm known as the Variational Quantum Eigensolver (VQE)[22] when applied to LiH_n complexes using an IBM quantum simulator, as well as results calculated using available classical electronic structure algorithms, and compare these to results obtained using full configuration interaction (FCI). Unlike other quantum algorithms meant for large scale quantum computers, for example Quantum Phase Estimation (QPE)[23], VQE can be utilized on a quantum simulator running on a computer workstation.

First introduced by Peruzzo et al. in 2013[22], VQE iteratively optimizes various parameterized quantum circuits that encode a desired wavefunction ansatz, and the quality of VQE calculations is directly related to the ansatz that is adopted. By parameterizing a wavefunction ansatz $\Psi(\vec{\theta})$, where $\vec{\theta}$ is a set of real valued parameters $\{\theta_i\}$, taken as a vector, the energy expectation value takes on the familiar form:

$$E(\vec{\theta}) = \langle \Psi(\vec{\theta}) | H | \Psi(\vec{\theta}) \rangle \tag{1}$$

where we have taken the wavefunction to be normalized and note that the expectation value is always larger than or equal to the lowest energy eigenvalue E_0 of the Hamiltonian, H, due to the variational principle. This allows one to optimize $\vec{\theta}$ using a classical computer in order to find an approximation to E_0. With the wavefunction stored on a quantum device, the energy expectation value (Eq. 1) is evaluated, allowing one to optimize the variational parameters of the wavefunction in order to determine a minimum E($\vec{\theta}$). It is through this approach and the belief that even minimal quantum resources could be useful when working in tandem with classical algorithms that has led to considerable interest in the use of VQE - like algorithms to simulate quantum systems[18,24–27].

In this study we apply VQE to LiH_n complexes including their singly charged cation and anion species. The choice of lithium hydride stems from the following: first, *LiH* is a simple molecule that requires at most 12 qubits when utilizing the minimal STO basis set[28] to represent its molecular orbitals (MOs) on a quantum simulator without any additional qubit reduction techniques such as application of the Parity mapper[29,30]. The MOs result from the $1s$, $2s$, $2p_x$, $2p_y$ and $2p_z$ atomic orbitals of lithium and the $1s$ atomic orbital from hydrogen, leading to a total of 6 MOs. When considering both up and down spin these give 12 qubits. A qualitative MO diagram for *LiH* is included (Figure 1). Secondly, lithium hydride has been used as a test molecule in many VQE benchmarking studies found in literature[31–34], though one will find no studies using VQE to investigate larger LiH_n, n = 2, 3, species as well as charged systems.

We therefore propose a quantum computational simulation study of LiH_n complexes as a means to investigate the capabilities of VQE through IBM's Qiskit library. Finally, since our main purpose at the National Energy Technology Laboratory (NETL) is to investigate problems that are energy related, it is relevant to note that lithium hydride, in its solid form, is involved in lithium-ion batteries, hydrogen storage, and even nuclear energy[31,35–42].

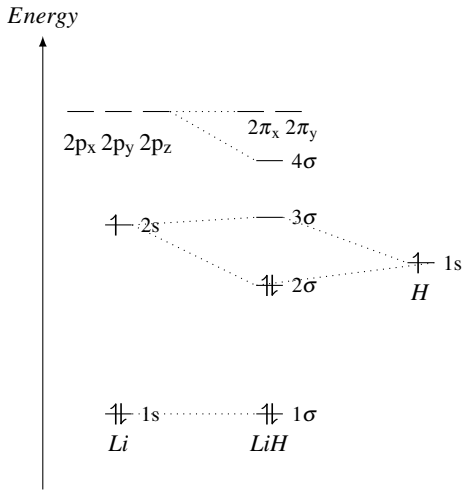

FIG. 1. MO diagram for *LiH*

II. METHODOLOGY AND COMPUTATIONAL DETAILS

A. VQE Calculations

The basic structure of the code used for our electronic structure calculations is adapted from Qiskit's electronic structure tutorial within their open-source second quantization framework Qiskit Nature[43]. Qiskit Nature supports the solving of quantum mechanical problems using quantum computing algorithms such as VQE. One can interface various classical electronic structure codes that find hartree fock (HF) solutions to the molecular many body Hamiltonian, and PySCF[44] is used for this purpose. The Gaussian type orbital STO-3G and STO-6G basis sets are used for the calculations[28].

Aspects of the VQE calculations that need to be specified by the user include choice of ansatz, mapper and optimizer. In addition to having already available wavefunction ansatzes, VQE allows the user to construct their own ansatz through the creation of a quantum circuit of their choosing, and many circuits have been developed by researchers for use in particular problem applications[45–47]. The ansatz used in our calculations uses a HF solution reference determinant when passed through a pre-defined unitary coupled cluster with singles and doubles (UCCSD) ansatz[48]. The resulting wavefunction now includes excitations to all orders beyond the single HF determinant, similar to coupled cluster (CC) singles plus doubles theory[49], and is used as $\langle\Psi(\vec{\theta})|$ within the VQE algorithm in minimizing the expectation given in Equation (1) with respect to the parameters represented by the vector $\vec{\theta}$.

The wavefunction is parameterized using the ansatz:

$$|\Psi(\vec{\theta})\rangle = e^{\hat{T}(\vec{\theta})-\hat{T}^{\dagger}(\vec{\theta})}|\Phi_0\rangle \tag{2}$$

where $|\Phi_0\rangle$ is the HF reference Slater determinant. The single and double components of the excitation operator $\hat{T}(\vec{\theta})$ in second quantized formalism can be written as:

$$\hat{T}_1(\vec{\theta}) = \sum_{i;a} \theta_i^a a_a^{\dagger} a_i \tag{3}$$

$$\hat{T}_2(\vec{\theta}) = \frac{1}{4} \sum_{i,j;a,b} \theta_{i,j}^{a,b} a_a^{\dagger} a_b^{\dagger} a_j a_i \tag{4}$$

with i and j indicating occupied orbitals, a and b indicating vacant orbitals, $a_i^{\dagger}$ and a_j corresponding to Fermionic creation and annihilation operators, respectfully. Summations are taken over all occupied and virtual orbitals. The collective vector of expansion coefficients $\vec{\theta}$ within the excitation operator is $\{\{\theta_i^a\},\{\theta_{i,j}^{a,b}\}\}$. The correlation energy is defined as the correction to the HF energy, and the ground state energy (E_{GS}) is defined by:

$$E_{GS} = E_{HF} + E_{UCCSD}^{corr}(\vec{\theta}_{min}) \tag{5}$$

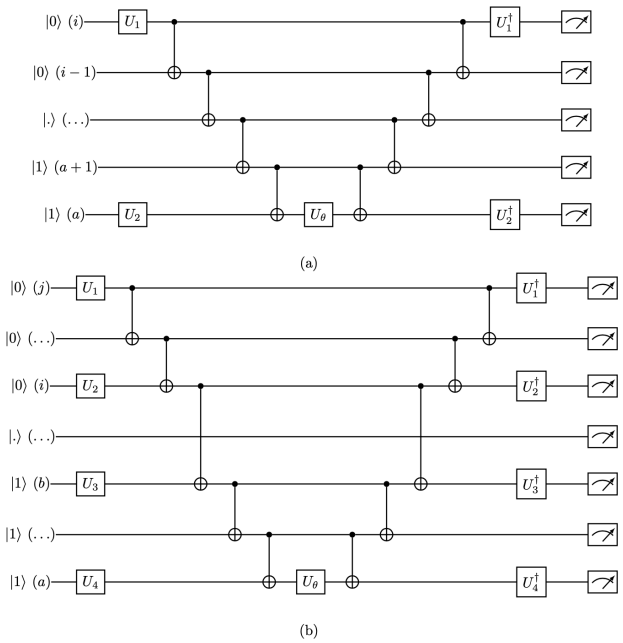

FIG. 2. (a) Single and (b) double excitation circuits corresponding to equations 4 and 5, respectfully. The arbitrary state $|.\rangle$ corresponds to $|1\rangle$ in the case it is occupied and $|0\rangle$ if it is vacant. In (a), CNOT gates applied to qubits $(i-1)$ through $(a+1)$ are repeated given an arbitrary number of qubits. Likewise, in (b) CNOT gates between occupied orbital qubits $(i,...,j)$ and virtual orbital qubits $(a,...,b)$ are repeated given use of an arbitrary number of occupied and virtual orbitals/qubits. Final qubit states are measured and circuit parameters are optimized classically. These are re-fed through the VQE algorithm until convergence in expectation value is reached.

Circuits for implementing the UCCSD trial wavefunction on the quantum simulator corresponding to the single (Equation 3) and double excitation operators (Equation 4) are shown in Figure 2[46,48]. Encoding the problem into the state of the quantum computer requires mapping the Fermionic operators onto spin operators, where each spin orbital is mapped onto a qubit, and the qubits follow spin statistics. The Jordan-Wigner transformation[50] is represented in Qiskit through the Jordan-Wigner Mapper. Initially developed for application to one-dimensional lattice models, the transformation recovers the true Fermionic anti-commutation relations observed for Fermionic creation and annihilation operators. One can show this transformation using unit-less Pauli spin matrices defined by Equations 6 - 8:

$$\sigma^x = \begin{pmatrix} 0 & 1 \\ 1 & 0 \end{pmatrix} \tag{6}$$

$$\sigma^y = \begin{pmatrix} 0 & -i \\ i & 0 \end{pmatrix} \tag{7}$$

$$\sigma^z = \begin{pmatrix} 1 & 0 \\ 0 & -1 \end{pmatrix} \tag{8}$$

Using these Pauli matrices, one can define spin $\frac{1}{2}$ Pauli ladder operators acting on a site j of a linear chain of spin particles as:

$$\sigma_j^+ = \frac{(\sigma_j^x + i\sigma_j^y)}{2} = f_j^\dagger \tag{9}$$

$$\sigma_j^- = \frac{(\sigma_j^x - i\sigma_j^y)}{2} = f_j \tag{10}$$

$$\sigma_j^z = 2f_j^\dagger f_j - 1 \tag{11}$$

From the definitions above, the anticommutator $\{\sigma_j^+, \sigma_j^-\} = 1$. From this, we now have the correct same site Fermionic relation in that $\{f_j^\dagger, f_j\} = 1$, but on different sites we have the commutator $[f_j^\dagger, f_k] = 0$, implying that spins on different sites commute. This is contrary to the nature of Fermions which anticommute when considering different sites. It is therefore necessary to define a new set of operators $l_j^\dagger$ and l_j:

$$l_j^\dagger = \exp(+i\pi \sum_{k=1}^{j-1} f_k^\dagger f_k) \cdot f_j^\dagger \tag{12}$$

$$l_j = \exp(-i\pi \sum_{k=1}^{j-1} f_k^\dagger f_k) \cdot f_j \tag{13}$$

$$l_j^\dagger l_j = f_j^\dagger f_j \tag{14}$$

These new operators differ from the previous definitions of $f_j^\dagger$ and f_j by a phase of $\exp(\pm i\pi \sum_{k=1}^{j-1} f_k^\dagger f_k)$, below written where the sum is taken as a product:

$$\prod_{k=1}^{j-1} \exp(\pm i\pi f_k^\dagger f_k) = \prod_{k=1}^{j-1} (1 - 2f_k^\dagger f_k) = \prod_{k=1}^{j-1} (-\sigma_k^z) \tag{15}$$

The transformed spin operators now have the appropriate Fermionic anticommutation relations that are valid within the spin statistics theorem, as well as their inverse transformations. Therefore the Jordan-Wigner mapping is complete. An additional mapper used is the Parity Mapper[29,30]. This mapping scheme uses a similar approach in converting the Fermionic operators to qubit spin operators but differs from Jordan-Wigner in that symmetry is introduced and exploited to reduce the size of the problem by two qubits. For example, neutral LiH calculated using the Jordan-Wigner Mapper requires 12 qubits when correlating all electrons, but use of the Parity mapper simplifies the calculation to only 10 qubits. The FreezeCoreTransformer command is included in calculations of all molecules to freeze core orbitals, further reducing the

complexity of the problem. The Parity orbital to qubit mapping scheme is used in all VQE calculations carried out in this study.

Once a parameterized variational circuit and adequate mapper are chosen, the parameters are optimized to minimize the expectation value of the target Hamiltonian. While multiple optimizers are available for use within Qiskit[51], VQE literature has suggested that when noise is not present, the Sequential Least Squares Quadratic Programming (SLSQP)[52] optimizer is best. The number of shots which represents the number of repetitions for sampling of each circuit used in VQE calculations is chosen to be the default of 1024, while the number of iterations performed within each calculation is set to 1000.

B. Gaussian and Molpro Calculations

Molecular geometries were obtained at the coupled cluster with singles plus doubles (CCSD) level using Gaussian16[53] with a frozen core approximation. These geometries were used in the VQE calculations. Molpro[54,55] is used to obtain corresponding frozen core FCI calculations. HF and CCSD results present in Figures 3 - 7 are computed using Gaussian at bond distance increments of 0.1Å . The same bond length increments are used in the VQE calculations. For dipole calculations of charged species, the origin is defined to be the center of nuclear charges.

III. RESULTS AND DISCUSSION

The reader is reminded that for systems in which only two electrons are correlated, calculated FCI properties are equivalent to CCSD. Therefore, for neutral LiH and for LiH_2^+, FCI values are omitted from respective figures and tables, and respective CCSD and UCCSD VQE results are used to compute relative ionization potentials and electron affinities. One will also notice that LiH^+ is absent within our study. This is because LiH^+ is a one electron problem in the frozen core approximation and there is no electron correlation. It would therefore be meaningless to study LiH^+ using a UCCSD ansatz as one would expect VQE calculations to be equal to HF. For this reason, we use LiH^+ HF results to calculate ionization potentials for LiH, as seen in Appendix A.

A. Applications to LiH Complexes

1. LiH

Figures 3 and 4 compare for LiH the energy and dipole curves produced through VQE using the UCCSD ansatz and the corresponding HF and CCSD results. From these figures it is seen that the VQE results correspond closely to those from CCSD. Electronic ground state properties for LiH reported in Table 1 agree with previously published data using the same basis sets at the CCSD level of theory[56]. Additionally, results displayed in Figures 3 and 4 agree with previously published VQE results on neutral LiH[31]. A shift in energy of approximately 0.1 Hartrees is observed when going from the STO-3G to STO-6G basis set, with a corresponding shift in the dipole moment of approximately 0.06 Debye.

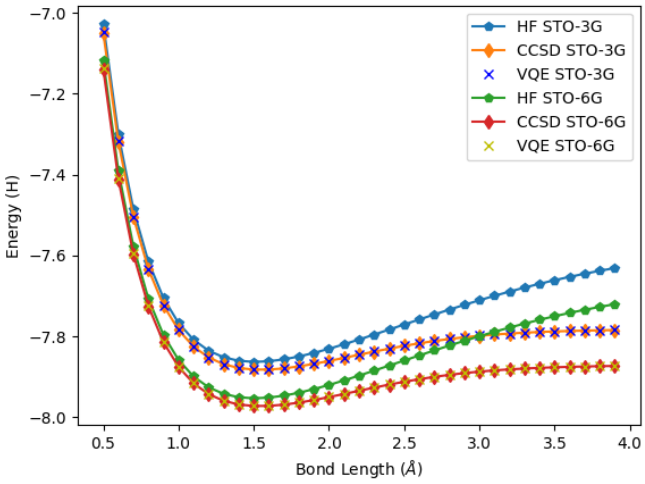

FIG. 3. Potential energy curve for lithium hydride obtained using various theoretical methods.

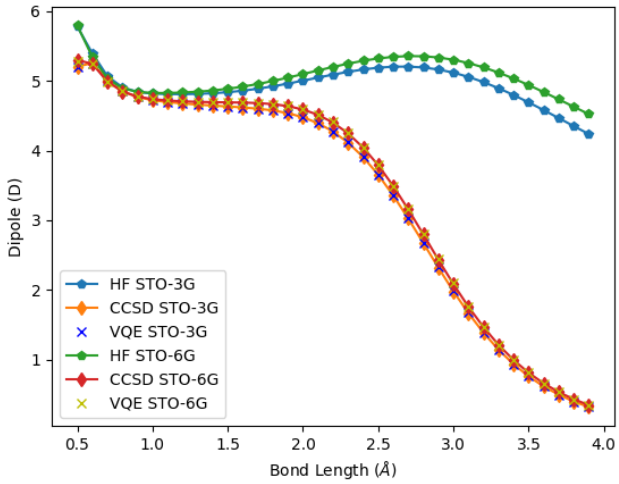

FIG. 4. Dipole moment curve for lithium hydride obtained using various theoretical methods.

2. LiH^-

LiH^- with three correlated electrons in the frozen core approximation allows us to compare CCSD and VQE results with those of FCI. Calculated properties through VQE are similar to those calculated using CCSD. It should be noted

TABLE I. *LiH* complex energies and dipoles. VQE energy and dipole moment use CCSD optimized geometry.

LiH STO-3G	CCSD Opt.	VQE	FCI
Energy (H)	-7.8825	-7.8825	n/a
Dipole (D)	4.63	4.63	n/a
LiH STO-6G	CCSD Opt.	VQE	FCI
Energy (H)	-7.9726	-7.9726	n/a
Dipole (D)	4.69	4.69	n/a

that the use of minimal basis sets for LiH^- results in an unbound electron, whereas with a sufficiently flexible basis set the excess electron would be bound[57]. In order to utilize larger, more diffuse basis sets, a significant increase in the ability for the classical computer to simulate qubits or algorithms which limit overall computational resources are required. CSSD and VQE STO-3G calculations provide an ionization potential of 0.2604 Hartrees, with STO-6G giving 0.2611 Hartrees as compared with 0.2822 Hartrees using CCSD/aug-cc-pVTZ[58,59]. Figures 6 and 7 compare CCSD, VQE and FCI dipole profiles for both STO-3G and STO-6G basis sets, respectfully. Both CCSD and VQE energies for LiH^- differ from FCI by less than 1 kcal/mol at both basis sets as can be seen from Table 2. Ionization potentials and electron affinities for *LiH* are presented in Table 3.

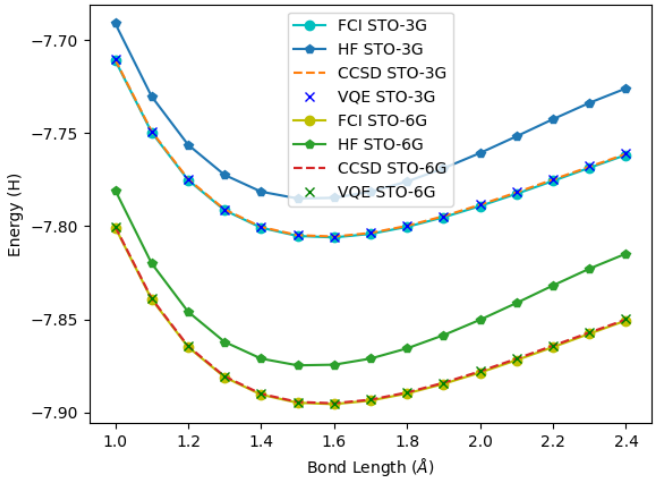

FIG. 5. Potential energy curve for lithium hydride anion obtained using various theoretical methods.

B. Applications to LiH_2 Complexes

When discussing results for the LiH_2 molecule, two geometries are considered. These are linear ($D_{\infty h}$ point group) and bent (C_{2v} point group). For the linear LiH_2 molecule, both the cation and anion are reported in addition to the neutral. However, for bent LiH_2 the optimization of the geometry of

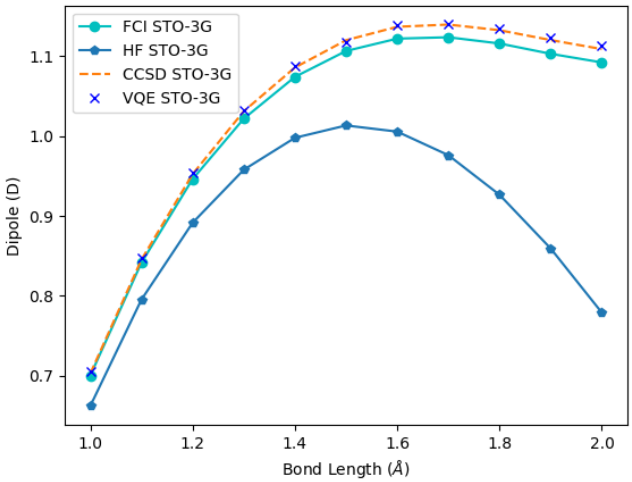

FIG. 6. Dipole moment curve for lithium hydride anion obtained using various theoretical methods at the STO-3G basis.

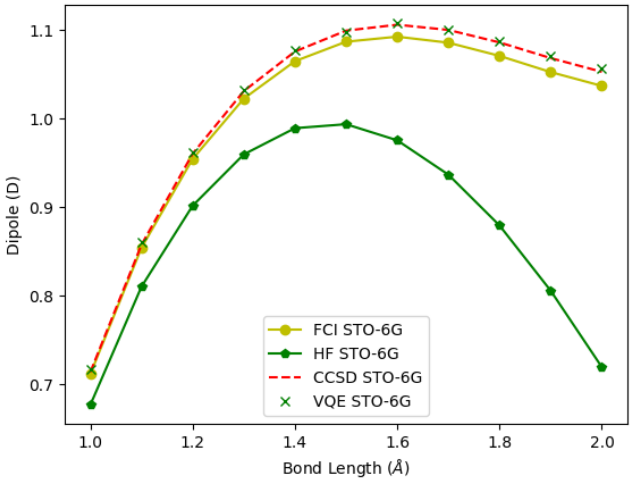

FIG. 7. Dipole moment curve for lithium hydride anion obtained using various theoretical methods at the STO-6G basis.

TABLE II. LiH^- complex energies and dipoles. VQE energy and dipole moment use CCSD optimized geometry.

LiH^- STO-3G	CCSD Opt.	VQE	FCI
Energy (H)	-7.8057	-7.8057	-7.8061
Dipole (D)	1.13	1.13	1.12
LiH^- STO-6G	CCSD Opt.	VQE	FCI
Energy (H)	-7.8952	-7.8952	-7.8957
Dipole (D)	1.11	1.11	1.09

the anion reverts to the linear structure, and for bent LiH_2 results are reported for only the neutral and the cation. Tabulated properties corresponding to linear and bent LiH_2 structures are

TABLE III. Ionization potential and electron affinity for LiH in units of Hartrees.

STO-3G	CCSD Opt.	VQE	FCI
Ionization Potential	0.2604	0.2604	0.2604
Electron Affinity	-0.0769	-0.0769	-0.0764
STO-6G	**CCSD Opt.**	**VQE**	**FCI**
Ionization Potential	0.2611	0.2611	0.2611
Electron Affinity	-0.0773	-0.0773	-0.0769

reported in Appendix B and C, respectively.

1. *Linear LiH_2 Complexes*

Linear neutral LiH_2 CCSD and VQE energies are similar in that they differ from FCI by approximately 4.5 and 4.6 kcal/mol, respectfully at the STO-3G basis. CCSD and VQE energies for linear neutral LiH_2 differ from FCI by approximately 4.1 kcal/mol at the STO-6G basis. Linear LiH_2^+ CCSD and VQE energies are similar using STO-3G, and differ by less than 1 kcal/mol at the STO-6G basis. Similarly, linear LiH_2^- CCSD and VQE energies differ from FCI by less than 1 kcal/mol at both basis sets. Differences in methods used can be seen from the ionization potentials and electron affinities shown in Table 8.

2. *Bent LiH_2 Complexes*

As can be seen in Appendix C, neutral bent LiH_2 CCSD and VQE energies differ from FCI by less than 1 kcal/mol at both minimal basis sets. For bent LiH_2^+ at the STO-3G basis, VQE dipole is 0.06 Debye lower than the CCSD result. Ionization potentials for bent LiH_2 using CCSD and VQE differ from FCI by less than 1 kcal/mol at both basis sets.

C. Applications to LiH_3 Complexes

Using both minimal basis sets, CCSD optimizations of LiH_3 complexes produce geometries that are of C_{2v} point group symmetry, with the exception of the anion which is of C_s point group symmetry. Calculated results for these LiH_3 complexes are reported within Appendix D. Energies and dipoles for neutral LiH_3 and LiH_3^+ complexes at both minimal basis sets using CCSD and VQE are consistent with those produced through FCI. As a result, ionization potentials for CCSD, VQE and FCI are similar at both minimal basis sets. FCI electron affinities, however, are slightly higher than that produced through both CCSD and VQE due to the additional electron correlation present within LiH_3^-, though this difference is less than 1 kcal/mol.

IV. VQE CALCULATION COST EVALUATION

The Parity mapper is known to be cost effective as it allows for a two qubit reduction compared to that of the Jordan-Wigner orbital to qubit mapping scheme. Figure 8 allows one to visualize differences in computational time using the STO-6G basis and either the Jordan-Wigner or Parity mapper, along with a frozen core approximation for increasingly large LiH_n systems. It can be seen when comparing Jordan-Wigner (blue) and Parity (green) mapping schemes without freezing core electrons for LiH_3 that a significant reduction in computational time is achieved when using the Parity mapper. The reduction in computational time with respect to mapper used becomes more extreme as the system increases in size. A similar argument can be made for both mappers when freezing core electrons, though the relative reduction in computational cost is not as extreme when correlating all electrons.

One explanation for this increase in computational time as the system size increases is the increased number of gates and large number of measurements per optimization step when using the UCCSD ansatz. One can deduce from this and Figure 8 that when running VQE there is poor scaling of the ansatz with respect to system size[18,60]. Given the gate model of quantum computing in which gates can act on only a few qubits at a time, the UCCSD operator needs to be simplified into a time ordered sequence of one and two particle operators using a Trotter expansion of the matrix exponential seen in Equation (2)[61]. Without use of this approximation, the UCCSD ansatz leads to an overall computational cost that is unfeasible given current NISQ hardware, not to mention the classical resources required within the hybrid VQE algorithm.

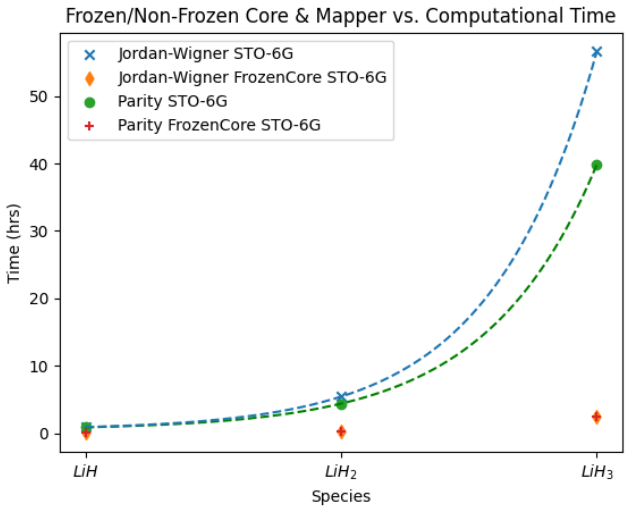

FIG. 8. VQE simulator calculation cost evaluation with respect to choice in orbital to qubit mapper and frozen core assumption.

V. CONCLUSION

As advancements in the development of a long-term quantum computer continues, current near-term NISQ devices, including quantum simulators, are available for use and further developments regarding these near-term devices are expected in the years to come[4,15,16]. However, without use of resource reduction algorithms, these near-term quantum devices are limited in the number of qubits they may represent, in turn limiting the complexity of systems that may be investigated using a quantum simulator. Current limitations in classical computational hardware only allow for the simulation of small quantum systems, and these are entirely dependent on the number of qubits that can be represented classically. As a result, current qubit limitations in quantum simulators restrict the size of the molecular system that may be studied. Additionally, use of more flexible basis sets to achieve higher accuracy results is also dependent on the number of available qubits in the quantum simulator.

We have investigated the quantum simulating capabilities of IBM Qiskit's VQE algorithm when used with available computational resources of various LiH_n complexes, including their singly charged ions. Generally, it is found that the electronic structure properties produced from CCSD and corresponding VQE calculations utilizing the UCCSD ansatz are similar when compared to FCI calculations. Without use of flexible bases, one is limited in accuracy when using VQE for more correlated systems. Additionally, we compare VQE calculation cost through the use of both Jordan-Wigner and Parity mapping schemes for the studied LiH_n species and provide an explanation as to the source of this poor scaling relationship as it pertains to the demand that increasingly larger systems have on the number of terms and operations required within the UCCSD ansatz.

To further advance the computational capabilities of NISQ devices and quantum simulators, algorithmic developments to allow for larger basis sets to be considered without a drastic increase in qubit number are needed. Techniques utilizing VQE and the UCCSD ansatz have been investigated and developed in which aspects of limited qubit connectivity, short coherence times and sizable gate error rates have been targeted to reduce the quantum resource requirements for electronic structure calculations. For example, Gagliardi et. al[14] has shown that through a combination of localized multireference wavefunctions with QPE and variational UCCSD, ground state energies can be calculated for molecules in which certain atoms use complex basis such as def2-svp and def2-tzvp. This is currently a very active area of research within the field of QC and QIS.

Further techniques that reduce computational resources include the adaptive derivative-assembled pseudo-trotter ansatz VQE method (ADAPT-VQE)[60,62] for ground and excited states, in which the algorithm is allowed to select its own compact quasi optimal ansatz through a selection process of systematically growing the ansatz by adding fermionic operators one at a time such that the maximal amount of correlation energy is recovered at each step iteration. Additional methods include correlation informed permutation of qubits (PERM-VQE)[63], qubit clustering (ClusterVQE)[64], and the use of a density matrix embedded theory (DMET)[65]. Using these techniques, we will be continuing our investigation of LiH_n complexes by considering various Li_xH_y complexes, as these particular species cannot be currently modeled using an unmodified VQE code given current qubit limitations. This will further aid in understanding of how VQE can be used to study and simulate energy relevant materials using near-term quantum devices[4,66].

SUPPLEMENTARY MATERIAL

See the supplementary material for optimized CCSD geometries of all LiH_n (n=1-3) species considered.

ACKNOWLEDGMENTS

The authors would like to thank Drs. Yueh-Lin Lee and Scott Crawford for their useful inputs and valuable discussions. This research used resources of the Oak Ridge Leadership Computing Facility, which is a DOE Office of Science User Facility supported under Contract DE-AC05-00OR22725.

This project was funded by the Department of Energy, through the Energy Efficiency and Renewable Energy Advanced Manufacturing Office Summer Internships Program at the National Energy Technology Laboratory an agency of the United States Government, through an appointment administered by the Oak Ridge Institute for Science and Education. Neither the United States Government nor any agency thereof, nor any of its employees, nor the support contractor, nor any of their employees, makes any warranty, expressor implied, or assumes any legal liability or responsibility for the accuracy, completeness, or usefulness of any information, apparatus, product, or process disclosed, or represents that its use would not infringe privately owned rights. Reference herein to any specific commercial product, process, or service by trade name, trademark, manufacturer, or otherwise does not necessarily constitute or imply its endorsement, recommendation, or favoring by the United States Government or any agency thereof. The views and opinions of authors expressed herein do not necessarily state or reflect those of the United States Government or any agency thereof.

AUTHOR DECLARATIONS

Conflict of Interest

The authors have no conflicts to disclose.

DATA AVAILABILITY STATEMENT

The data that support the findings of this study are available within the article. Optimized CCSD geometries at both min-

imal basis sets for all species considered are presented in the supplementary material.

Appendix A: LiH^+ Hartree Fock Energies and Dipoles

TABLE IV. Energy and dipole moment use HF optimized geometry.

LiH^+ STO-3G	HF Opt.
Energy (H)	-7.6222
Dipole (D)	1.71
LiH^+ STO-6G	HF Opt.
Energy (H)	-7.7115
Dipole (D)	1.73

Appendix B: Linear LiH_2 Complex Energies, Ionization Potentials and Electron Affinities

TABLE V. VQE energy uses CCSD optimized geometry.

LiH_2 STO-3G	CCSD Opt.	VQE	FCI
Energy (H)	-8.3533	-8.3532	-8.3605
LiH_2 STO-6G	CCSD Opt.	VQE	FCI
Energy (H)	-8.4474	-8.4474	-8.4540

TABLE VI. VQE energy uses CCSD optimized geometry.

LiH_2^+ STO-3G	CCSD Opt.	VQE	FCI
Energy (H)	-8.1093	-8.1093	n/a
LiH_2^+ STO-6G	CCSD Opt.	VQE	FCI
Energy (H)	-8.2020	-8.2021	n/a

TABLE VII. VQE energy uses CCSD optimized geometry.

LiH_2^- STO-3G	CCSD Opt.	VQE	FCI
Energy (H)	-8.4077	-8.4077	-8.4081
LiH_2^- STO-6G	CCSD Opt.	VQE	FCI
Energy (H)	-8.5028	-8.5028	-8.5032

TABLE VIII. Ionization potential and electron affinity for linear LiH_2 in units of Hartrees.

STO-3G	CCSD Opt.	VQE	FCI
Ionization Potential	0.2440	0.2439	0.2512
Electron Affinity	0.0544	0.0545	0.0476
STO-6G	CCSD Opt.	VQE	FCI
Ionization Potential	0.2454	0.2453	0.2519
Electron Affinity	0.0554	0.0554	0.0492

Appendix C: Bent LiH_2 Complex Energies, Dipoles and Ionization Potentials

TABLE IX. VQE energy and dipole moment use CCSD optimized geometry.

LiH_2 STO-3G	CCSD Opt.	VQE	FCI
Energy (H)	-8.3760	-8.3759	-8.3763
Dipole (D)	3.11	3.11	3.10
LiH_2 STO-6G	CCSD Opt.	VQE	FCI
Energy (H)	-8.4699	-8.4698	-8.4702
Dipole (D)	3.17	3.17	3.16

TABLE X. VQE energy and dipole moment use CCSD optimized geometry.

LiH_2^+ STO-3G	CCSD Opt.	VQE	FCI
Energy (H)	-8.2805	-8.2805	n/a
Dipole (D)	3.70	3.64	n/a
LiH_2^+ STO-6G	CCSD Opt.	VQE	FCI
Energy (H)	-8.3742	-8.3742	n/a
Dipole (D)	3.74	3.74	n/a

TABLE XI. Ionization potential for bent LiH_2 in units of Hartrees.

STO-3G	CCSD Opt.	VQE	FCI
Ionization Potential	0.0955	0.0954	0.0958
STO-6G	CCSD Opt.	VQE	FCI
Ionization Potential	0.0957	0.0956	0.0960

Appendix D: LiH_3 Complex Energies, Dipoles, Ionization Potentials and Electron Affinities

TABLE XII. VQE energy and dipole moment use CCSD optimized geometry.

LiH_3 STO-3G	CCSD Opt.	VQE	FCI
Energy (H)	-9.0242	-9.0242	-9.0242
Dipole (D)	4.94	4.94	4.94
LiH_3 STO-6G	CCSD Opt.	VQE	FCI
Energy (H)	-9.1223	-9.1223	-9.1224
Dipole (D)	4.97	4.97	4.97

TABLE XIII. VQE energy and dipole moment use CCSD optimized geometry.

LiH_3^+ STO-3G	CCSD Opt.	VQE	FCI
Energy (H)	-8.7675	-8.7675	-8.7675
Dipole (D)	2.07	2.07	2.07
LiH_3^+ STO-6G	CCSD Opt.	VQE	FCI
Energy (H)	-8.8646	-8.8646	-8.8646
Dipole (D)	2.08	2.08	2.08

TABLE XIV. VQE energy and dipole moment use CCSD optimized geometry.

LiH_3^- STO-3G	CCSD Opt.	VQE	FCI
Energy (H)	-8.9436	-8.9436	-8.9440
Dipole (D)	8.35	8.35	8.36
LiH_3^- STO-6G	CCSD Opt.	VQE	FCI
Energy (H)	-9.0418	-9.0418	-9.0422
Dipole (D)	8.42	8.42	8.42

TABLE XV. Ionization potential and electron affinity for LiH_3 in units of Hartrees.

STO-3G	CCSD Opt.	VQE	FCI
Ionization Potential	0.2567	0.2567	0.2567
Electron Affinity	-0.0806	-0.0806	-0.0802
STO-6G	CCSD Opt.	VQE	FCI
Ionization Potential	0.2577	0.2577	0.2578
Electron Affinity	-0.0806	-0.0806	-0.0801

REFERENCES

[1] S. Grimme and P. R. Schreiner, "Computational chemistry: the fate of current methods and future challenges," Angewandte Chemie International Edition **57**, 4170–4176 (2018).

[2] M. A. Nielsen and I. Chuang, "Quantum computation and quantum information," (2002).

[3] R. P. Feynman, "Simulating physics with computers, 1981," International Journal of Theoretical Physics **21** (1981).

[4] H. P. Paudel, M. Syamlal, S. E. Crawford, Y.-L. Lee, R. A. Shugayev, P. Lu, P. R. Ohodnicki, D. Mollot, and Y. Duan, "Quantum computing and simulations for energy applications: Review and perspective," ACS Engineering Au (2022), 10.1021/acsengineeringau.1c00033.

[5] Y. Cao, J. Romero, J. P. Olson, M. Degroote, P. D. Johnson, M. Kieferová, I. D. Kivlichan, T. Menke, B. Peropadre, N. P. Sawaya, S. Sim, L. Veis, and A. Aspuru-Guzik, "Quantum chemistry in the age of quantum computing," (2019).

[6] D. Deutsch, "Quantum theory, the church–turing principle and the universal quantum computer," Proceedings of the Royal Society of London. A. Mathematical and Physical Sciences **400**, 97–117 (1985).

[7] D. Deutsch and R. Jozsa, "Rapid solution of problems by quantum computation," Proceedings of the Royal Society of London. Series A: Mathematical and Physical Sciences **439**, 553–558 (1992).

[8] E. Bernstein and U. Vazirani, "Quantum complexity theory," SIAM Journal on computing **26**, 1411–1473 (1997).

[9] P. W. Shor, "Algorithms for quantum computation: discrete logarithms and factoring," in *Proceedings 35th annual symposium on foundations of computer science* (Ieee, 1994) pp. 124–134.

[10] L. K. Grover, "A fast quantum mechanical algorithm for database search," in *Proceedings of the twenty-eighth annual ACM symposium on Theory of computing* (1996) pp. 212–219.

[11] S. Lloyd, "Universal quantum simulators," Science **273**, 1073–1078 (1996).

[12] C. Park, U. Kim, C. J. Ju, J. S. Park, Y. M. Kim, and K. Char, "High mobility field effect transistor based on basno3 with al2o3 gate oxide," Applied Physics Letters **105**, 203503 (2014).

[13] V.-P. Lauzon, "Quantum computing - how does it scale?" (2018), `https://vincentlauzon.com/2018/03/21/quantum-computing-how-does-it-scale/`.

[14] M. Otten, M. R. Hermes, R. Pandharkar, Y. Alexeev, S. K. Gray, and L. Gagliardi, "Localized quantum chemistry on quantum computers," Journal of Chemical Theory and Computation **18**, 7205–7217 (2022).

[15] P. Ball, "First quantum computer to pack 100 qubits enters crowded race," Nature **599**, 542 (2021).

[16] H. Collins and C. Nay, "Ibm unveils 400 qubit-plus quantum processor and next-generation ibm quantum system two. company outlines path towards quantum-centric supercomputing with new hardware, software, and system breakthrough," newsroom.ibm.com (2022).

[17] K. Bharti, A. Cervera-Lierta, T. H. Kyaw, T. Haug, S. Alperin-Lea, A. Anand, M. Degroote, H. Heimonen, J. S. Kottmann, T. Menke, *et al.*, "Noisy intermediate-scale quantum (nisq) algorithms," arXiv preprint arXiv:2101.08448 (2021).

[18] H. Liu, G. H. Low, D. S. Steiger, T. Häner, M. Reiher, and M. Troyer, "Prospects of quantum computing for molecular sciences," (2021), 10.1186/s41313-021-00039-z.

[19] "Vqe — qiskit 0.36.2 documentation," `https://qiskit.org/documentation/stubs/qiskit.algorithms.VQE.html`.

[20] G. Van Rossum and F. L. Drake, *Python 3 Reference Manual* (CreateSpace, Scotts Valley, CA, 2009).

[21] M. T. Nguyen, Y.-L. Lee, D. Alfonso, Q. Shao, and Y. Duan, "Description of reaction and vibrational energetics of co2–nh3 interaction using quantum computing algorithms," AVS Quantum Science **5** (2023).

[22] A. Peruzzo, J. McClean, P. Shadbolt, M.-H. Yung, X.-Q. Zhou, P. J. Love, A. Aspuru-Guzik, and J. L. O'Brien, "A variational eigenvalue solver on a quantum processor," (2013), 10.1038/ncomms5213.

[23] D. S. Abrams and S. Lloyd, "Quantum algorithm providing exponential speed increase for finding eigenvalues and eigenvectors," Physical Review Letters **83**, 5162 (1999).

[24] J. R. McClean, J. Romero, R. Babbush, and A. Aspuru-Guzik, "The theory of variational hybrid quantum-classical algorithms," New Journal of

Physics **18** (2016), 10.1088/1367-2630/18/2/023023.
[25] T. E. O'Brien, B. Senjean, R. Sagastizabal, X. Bonet-Monroig, A. Dutkiewicz, F. Buda, L. DiCarlo, and L. Visscher, "Calculating energy derivatives for quantum chemistry on a quantum computer," npj Quantum Information **5** (2019), 10.1038/s41534-019-0213-4.
[26] P. Lolur, M. Rahm, M. Skogh, L. García-Álvarez, and G. Wendin, "Benchmarking the variational quantum eigensolver through simulation of the ground state energy of prebiotic molecules on high-performance computers," (2020), 10.1063/5.0054915.
[27] A. Anaya and F. Delgado, "Simulating molecules using the vqe algorithm on qiskit," arXiv preprint arXiv:2201.04216 (2022).
[28] W. J. Hehre, R. F. Stewart, and J. A. Pople, "Self-consistent molecular-orbital methods. i. use of gaussian expansions of slater-type atomic orbitals," The Journal of Chemical Physics **51**, 2657–2664 (1969).
[29] S. B. Bravyi and A. Y. Kitaev, "Fermionic quantum computation," Annals of Physics **298**, 210–226 (2002).
[30] J. T. Seeley, M. J. Richard, and P. J. Love, "The bravyi-kitaev transformation for quantum computation of electronic structure," The Journal of chemical physics **137**, 224109 (2012).
[31] J. E. Rice, T. P. Gujarati, M. Motta, T. Y. Takeshita, E. Lee, J. A. Latone, and J. M. Garcia, "Quantum computation of dominant products in lithium-sulfur batteries," Journal of Chemical Physics **154** (2021), 10.1063/5.0044068.
[32] H. Chen, M. Nusspickel, J. Tilly, G. H. Booth, *et al.*, "Variational quantum eigensolver for dynamic correlation functions," Physical Review A **104**, 032405 (2021).
[33] M. Ostaszewski, E. Grant, and M. Benedetti, "Structure optimization for parameterized quantum circuits," Quantum **5**, 391 (2021).
[34] S. E. Rasmussen, N. J. S. Loft, T. Bækkegaard, M. Kues, and N. T. Zinner, "Reducing the amount of single-qubit rotations in vqe and related algorithms," Advanced Quantum Technologies **3**, 2000063 (2020).
[35] H. Zhang, S. Ju, G. Xia, and X. Yu, "Identifying the positive role of lithium hydride in stabilizing li metal anodes," Science advances **8**, eabl8245 (2022).
[36] F. H. Welch, "Lithium hydride: a space age shielding material," Nuclear Engineering and Design **26**, 444–460 (1974).
[37] L. Wang, M. Z. Quadir, and K.-F. Aguey-Zinsou, "Direct and reversible hydrogen storage of lithium hydride (lih) nanoconfined in high surface area graphite," International Journal of Hydrogen Energy **41**, 18088–18094 (2016).
[38] B. Cassenti, "Lithium hydride in nuclear pulse propulsion," in *38th AIAA/ASME/SAE/ASEE Joint Propulsion Conference & Exhibit* (2002) p. 3930.
[39] C. Laasch, "Chemists prove the existence of lih in battery," Brookhaven National Laboratory Newsroom - Media Communications (2021).
[40] Y. Oumellal, A. Rougier, G. Nazri, J. Tarascon, and L. Aymard, "Metal hydrides for lithium-ion batteries," Nature materials **7**, 916–921 (2008).
[41] S. Kim, H. Oguchi, N. Toyama, T. Sato, S. Takagi, T. Otomo, D. Arunkumar, N. Kuwata, J. Kawamura, and S.-i. Orimo, "A complex hydride lithium superionic conductor for high-energy-density all-solid-state lithium metal batteries," Nature communications **10**, 1081 (2019).
[42] M. N. Guzik, R. Mohtadi, and S. Sartori, "Lightweight complex metal hydrides for li-, na-, and mg-based batteries," Journal of Materials Research **34**, 877–904 (2019).
[43] "Qiskit nature tutorials," `https://qiskit.org/documentation/nature/tutorials/index.html`.
[44] Q. Sun, T. C. Berkelbach, N. S. Blunt, G. H. Booth, S. Guo, Z. Li, J. Liu, J. D. McClain, E. R. Sayfutyarova, S. Sharma, *et al.*, "Pyscf: the python-based simulations of chemistry framework," Wiley Interdisciplinary Reviews: Computational Molecular Science **8**, e1340 (2018).
[45] A. Asthana, A. Kumar, V. Abraham, H. Grimsley, Y. Zhang, L. Cincio, S. Tretiak, P. A. Dub, S. E. Economou, E. Barnes, *et al.*, "Equation-of-motion variational quantum eigensolver method for computing molecular excitation energies, ionization potentials, and electron affinities," arXiv preprint arXiv:2206.10502 (2022).
[46] P. K. Barkoutsos, J. F. Gonthier, I. Sokolov, N. Moll, G. Salis, A. Fuhrer, M. Ganzhorn, D. J. Egger, M. Troyer, A. Mezzacapo, *et al.*, "Quantum algorithms for electronic structure calculations: Particle-hole hamiltonian and optimized wave-function expansions," Physical Review A **98**, 022322 (2018).
[47] P. J. Ollitrault, A. Baiardi, M. Reiher, and I. Tavernelli, "Hardware efficient quantum algorithms for vibrational structure calculations," Chemical science **11**, 6842–6855 (2020).
[48] J. Romero, R. Babbush, J. R. McClean, C. Hempel, P. J. Love, and A. Aspuru-Guzik, "Strategies for quantum computing molecular energies using the unitary coupled cluster ansatz," Quantum Science and Technology **4**, 014008 (2018).
[49] M. R. Hoffmann and J. Simons, "A unitary multiconfigurational coupled-cluster method: Theory and applications," The Journal of chemical physics **88**, 993–1002 (1988).
[50] P. Jordan and E. P. Wigner, "Über das paulische äquivalenzverbot," in *The Collected Works of Eugene Paul Wigner* (Springer, 1993) pp. 109–129.
[51] W. Lavrijsen, A. Tudor, J. Müller, C. Iancu, and W. De Jong, "Classical optimizers for noisy intermediate-scale quantum devices," in *2020 IEEE international conference on quantum computing and engineering (QCE)* (IEEE, 2020) pp. 267–277.
[52] P. T. Boggs and J. W. Tolle, "Sequential quadratic programming," Acta numerica **4**, 1–51 (1995).
[53] M. J. Frisch, G. W. Trucks, H. B. Schlegel, G. E. Scuseria, M. A. Robb, J. R. Cheeseman, G. Scalmani, V. Barone, G. A. Petersson, H. Nakatsuji, X. Li, M. Caricato, A. V. Marenich, J. Bloino, B. G. Janesko, R. Gomperts, B. Mennucci, H. P. Hratchian, J. V. Ortiz, A. F. Izmaylov, J. L. Sonnenberg, D. Williams-Young, F. Ding, F. Lipparini, F. Egidi, J. Goings, B. Peng, A. Petrone, T. Henderson, D. Ranasinghe, V. G. Zakrzewski, J. Gao, N. Rega, G. Zheng, W. Liang, M. Hada, M. Ehara, K. Toyota, R. Fukuda, J. Hasegawa, M. Ishida, T. Nakajima, Y. Honda, O. Kitao, H. Nakai, T. Vreven, K. Throssell, J. A. Montgomery, Jr., J. E. Peralta, F. Ogliaro, M. J. Bearpark, J. J. Heyd, E. N. Brothers, K. N. Kudin, V. N. Staroverov, T. A. Keith, R. Kobayashi, J. Normand, K. Raghavachari, A. P. Rendell, J. C. Burant, S. S. Iyengar, J. Tomasi, M. Cossi, J. M. Millam, M. Klene, C. Adamo, R. Cammi, J. W. Ochterski, R. L. Martin, K. Morokuma, O. Farkas, J. B. Foresman, and D. J. Fox, "Gaussian~16 Revision C.01," (2016), gaussian Inc. Wallingford CT.
[54] H.-J. Werner, P. J. Knowles, G. Knizia, F. R. Manby, and M. Schütz, "Molpro: a general-purpose quantum chemistry program package," Wiley Interdisciplinary Reviews: Computational Molecular Science **2**, 242–253 (2012).
[55] H.-J. Werner, P. J. Knowles, F. R. Manby, J. A. Black, K. Doll, A. Heßelmann, D. Kats, A. Köhn, T. Korona, D. A. Kreplin, *et al.*, "The molpro quantum chemistry package," The Journal of chemical physics **152** (2020).
[56] V. E. Elfving, M. Millaruelo, J. A. Gámez, and C. Gogolin, "Simulating quantum chemistry in the seniority-zero space on qubit-based quantum computers," Physical Review A **103**, 032605 (2021).
[57] A. Szabo and N. S. Ostlund, *Modern quantum chemistry: introduction to advanced electronic structure theory* (Courier Corporation, 2012).
[58] B. P. Prascher, D. E. Woon, K. A. Peterson, T. H. Dunning, and A. K. Wilson, "Gaussian basis sets for use in correlated molecular calculations. vii. valence, core-valence, and scalar relativistic basis sets for li, be, na, and mg," Theoretical Chemistry Accounts **128**, 69–82 (2011).
[59] T. H. Dunning Jr, "Gaussian basis sets for use in correlated molecular calculations. i. the atoms boron through neon and hydrogen," The Journal of chemical physics **90**, 1007–1023 (1989).
[60] H. R. Grimsley, S. E. Economou, E. Barnes, and N. J. Mayhall, "An adaptive variational algorithm for exact molecular simulations on a quantum computer," Nature Communications **10** (2019), 10.1038/s41467-019-10988-2.
[61] N. Hatano and M. Suzuki, "Finding exponential product formulas of higher orders," Quantum Annealing and Other Optimization Methods, Eds. A. Das and B.K. Chakrabarti , 37–68 (2005).
[62] A. Kumar, A. Asthana, C. Masteran, E. F. Valeev, Y. Zhang, L. Cincio, S. Tretiak, and P. A. Dub, "Accurate quantum simulation of molecular ground and excited states with a transcorrelated hamiltonian," arXiv preprint arXiv:2201.09852 (2022).
[63] N. V. Tkachenko, J. Sud, Y. Zhang, S. Tretiak, P. M. Anisimov, A. T. Arrasmith, P. J. Coles, L. Cincio, and P. A. Dub, "Correlation-informed permutation of qubits for reducing ansatz depth in the variational quantum eigensolver," PRX Quantum **2**, 020337 (2021).
[64] Y. Zhang, L. Cincio, C. F. Negre, P. Czarnik, P. J. Coles, P. M. Anisimov, S. M. Mniszewski, S. Tretiak, and P. A. Dub, "Variational quantum eigensolver with reduced circuit complexity," npj Quantum Information **8**, 1–10

(2022).
[65]G. Greene-Diniz, D. Z. Manrique, W. Sennane, Y. Magnin, E. Shishenina, P. Cordier, P. Llewellyn, M. Krompiec, M. J. Rančić, and D. M. Ramo, "Modelling carbon capture on metal-organic frameworks with quantum computing," arXiv preprint arXiv:2203.15546 (2022).
[66]S. Bush, Y. Duan, B. Gilbert, A. Hussey, J. Levy, D. Miller, R. Pooser, and M. Syamlal, "Fossil energy workshop on quantum information science & technology (summary report)," Tech. Rep. (National Energy Technology Laboratory (NETL), Pittsburgh, PA, Morgantown, WV . . . , 2020).

Supplementary Materials for

Ground State Property Calculations of LiH_n Complexes using IBM Qiskit's Quantum Simulator

[1,2]Benjamin Avramidis, [3]Hari P. Paudel, [1]Dominic Alfonso, [1]Yuhua Duan and [2]Kenneth D. Jordan

[1]National Energy Technology Laboratory, United States Department of Energy, Pittsburgh, PA 15236, USA
[2]Department of Chemistry, University of Pittsburgh, 219 Parkman Ave, Pittsburgh, PA 15213, USA
[3]NETL Support Contractor, 626 Cochrans Mill Road, Pittsburgh, PA 15236-0940, USA

I CCSD Optimized Geometries for LiH species

I.I LiH

(**STO-3G**)

Li: (-0.0181804602, 0.0, 0.0)
H: (1.5291804602, 0.0, 0.0)

(**STO-6G**)

Li: (-0.0155210221, 0.0, 0.0)
H: (1.5265210221, 0.0, 0.0)

I.II LiH^+

(**STO-3G (HF)**)

Li: (-0.2299643487, 0.0, 0.0)
H: (1.7409643487, 0.0 ,0.0)

(**STO-6G (HF)**)

Li: (-0.2294820094, 0.0, 0.0)
H: (1.7404820094, 0.0, 0.0)

I.III LiH^-

(**STO-3G**)

Li: (0.0, 0.0, 0.0)
H: (0.0, 0.0, 1.5725122996)

(**STO-6G**)

Li: (0.0, 0.0, 0.0)
H: (0.0, 0.0, 1.5725122996)

II CCSD Optimized Geometries for LiH_2 species

II.I Linear LiH_2 species

II.I.1 LiH_2

(**STO-3G**)

Li: (0.0, 0.0, 0.0)
H: (-1.6293765778, 0.0, 0.0)
H: (1.6293765778, 0.0, 0.0)

(**STO-6G**)

Li: (0.0, 0.0, 0.0)
H: (-1.6270122456, 0.0, 0.0)
H: (1.6270122456, 0.0, 0.0)

II.I.2 LiH_2^+

(**STO-3G**)

Li: (0.0, 0.0, 0.0)
H: (-1.9573612681, 0.0, 0.0)
H: (1.9573612681, 0.0, 0.0)

(**STO-6G**)

Li: (0.0, 0.0, 0.0)
H: (-1.9567977051, 0.0, 0.0)
H: (1.9567977051, 0.0, 0.0)

II.I.3 LiH_2^-

(**STO-3G**)

Li: (0.0, 0.0, 0.0)
H: (-1.5657047531, 0.0, 0.0)
H: (1.5657047531, 0.0, 0.0)

(**STO-6G**)

Li: (0.0, 0.0, 0.0)
H: (-1.5630266789, 0.0, 0.0)
H: (1.5630266789, 0.0, 0.0)

II.II Bent LiH_2 species

II.II.1 LiH_2

(**STO-3G**)

Li: (0.0, 0.437825141, 0.0)
H: (-1.007046968, -0.8119125705, 0.0)
H: (1.007046968, -0.8119125705, 0.0)

(**STO-6G**)

Li: (0.0, 0.4412360228, 0.0)
H: (-0.9914512018, -0.8136180114, 0.0)
H: (0.9914512018, -0.8136180114, 0.0)

II.II.2 LiH_2^+

(**STO-3G**)

Li: (0.0, 0.0, 0.8420498482)
H: (0.0, 0.3816787774, -1.2962249241)
H: (0.0, -0.3816787774, -1.2962249241)

(**STO-6G**)

Li: (0.0, 0.0, 0.843094854)
H: (0.0, 0.3796867668, -1.296747427)
H: (0.0, -0.3796867668, -1.296747427)

III CCSD Optimized Geometries for LiH_3 species

III.I LiH_3

(**STO-3G**)

Li: (0.0, 0.5742701053, 0.0)
H: (0.3761690813, -1.5964314188, 0.0)
H: (-0.3761690813, -1.5964314188, 0.0)
H: (0.0, 2.1185927323, 0.0)

(**STO-6G**)

Li: (0.0, 0.5745285121, 0.0)
H: (0.3745515758, -1.5943364696, 0.0)
H: (-0.3745515758, -1.5943364696, 0.0)
H: (0.0, 2.1141444271, 0.0)

III.II LiH_3^+

(**STO-3G**)

Li: (0.0, 0.4458857224, 0.0)
H: (0.3817589841, -1.6774498429, 0.0)
H: (-0.3817589841, -1.6774498429, 0.0)
H: (0.0, 2.4090139635, 0.0)

(**STO-6G**)

Li: (0.0, 0.4465585922, 0.0)
H: (0.3797140817, -1.6774541354, 0.0)
H: (-0.3797140817, -1.6774541354, 0.0)
H: (0.0, 2.4083496785, 0.0)

III.III LiH_3^-

(**STO-3G**)

Li: (0.2465964441, 1.905175701, 0.0)
H: (-0.3380784609, -2.6637884691, 0.0)
H: (-0.0022944938, 0.3511846717, 0.0)
H: (-0.4256234895, -3.3942719036, 0.0)

(**STO-6G**)

Li: (0.2521885944, 1.9319746217, 0.0)
H: (-0.3411785343, -2.6925658902, 0.0)
H: (-0.0022022611, 0.3800456265, 0.0)
H: (-0.428207799, -3.421154358, 0.0)